Journal of Cardiovascular Magnetic Resonance®, 3(3), 195–208 (2001)

Myocardial Viability: Magnetic Resonance Assessment of Functional Reserve and Tissue Characterization

Norbert Watzinger, Maythem Saeed, Michael F. Wendland, Haydar Akbari, Gunnar Lund, and Charles B. Higgins

Department of Radiology, University of California, San Francisco, California

ABSTRACT

The determination of myocardial viability is crucial in patients with left ventricular dysfunction resulting from acute myocardial ischemia or chronic coronary artery disease. Viable myocardium will most likely benefit from revascularization procedures. However, the revascularization of scar tissue will not lead to improvement of ventricular function and furthermore bears unnecessary risk for the patient. Currently, echocardiographic and radionuclide techniques are the most established methods for the assessment of presence and extent of viable myocardium. Magnetic resonance imaging (MRI) also provides multiple approaches for determining viability of acute ischemically injured and hibernating myocardium. MRI can assess contractile reserve in a manner similar to echocardiography. Additionally, contrast-enhanced MRI can characterize myocardial ischemic injury, including the ability to discriminate viable from nonviable zones. Several new contrast media have been introduced for this purpose. This review addresses the progress toward the goal of defining myocardial viability based on MR techniques and focuses on the current and future role of MR in the assessment of viable myocardium.

Key Words: *Coronary heart disease; MR imaging; Myocardial viability*

Address correspondence and reprint requests to Charles B. Higgins.

INTRODUCTION

''Hibernating'' can be described as a condition of chronic hypoperfusion leading to down-regulation of myocardial contractility and resulting in impaired left ventricular (LV) function (1). After revascularization, which reestablishes adequate blood supply, these areas are capable of restoring their normal contractile function. Therefore, it is reasonable that the assessment of hibernating myocardium could allow a better estimation of risks and benefits in patients with LV dysfunction who are scheduled for a revascularization procedure (2).

On the other hand, after an acute ischemic injury the recovery of contraction may be delayed despite reperfusion, a condition called ''stunning'' (3). Stunned myocardium recovers spontaneously after restoration of blood flow. The time course of recovery depends on the duration of ischemia, and dysfunction may be present for several days, although coronary blood flow is normal (4).

Stunning, hibernation, and necrosis may coexist in the clinical setting of ischemia. Therefore, the assessment of the presence and extent of viable myocardium is of considerable clinical importance to determine prognosis and to guide therapeutic interventions in patients with recurrent angina, previous myocardial infarction, or LV dysfunction. Several techniques, including dobutamine echocardiography, single photon emission tomography (SPECT), and positron emission tomography (PET), have been used to predict myocardial viability. These methods demonstrate residual function, perfusion, or metabolism in dysfunctional myocardium. However, functional improvement after restoration of adequate perfusion must be regarded as the clinical gold standard (5).

The usefulness of magnetic resonance (MR) techniques in the evaluation of ischemic heart disease has been demonstrated for more than 15 years. More recently, several promising approaches to assess myocardial viability have been described (6,7). In addition to the depiction of myocardial anatomy, function and functional reserve MR has the capability to determine myocardial perfusion, cell membrane integrity, and cell metabolism, making it a potentially comprehensive noninvasive imaging modality. This review focuses on the current and future role of MR techniques in the assessment of myocardial viability using approaches directed at assessing functional reserve and tissue characterization to discriminate between viable and nonviable myocardium.

ASSESSMENT OF FUNCTIONAL RESERVE

In the setting of myocardial infarction, structural changes take place and scar formation is completed after 3–4 months (8). In acute stages of an ischemic event, nonviable and viable myocardium may have the same gross appearance in terms of wall thickness and absence of resting function. Therefore, observing anatomy and resting function in the acute setting by spin echo (SE) or gradient recalled echo (GRE) MR techniques is not helpful to determine viability (9).

After several weeks, infarcted myocardium shows wall thinning and decreased signal intensity on SE imaging consistent with scar formation (10,11). On the other hand, in the setting of chronic myocardial infarction or chronic coronary artery disease with LV dysfunction, it has been shown that preserved diastolic wall thickness $\geq$5.5 mm and systolic wall thickening $\geq$1 mm at baseline MR imaging (MRI) are associated with viability classified by SPECT or PET (12,13). It has also been asserted that several months after infarction, an end-systolic wall thickness $>$8.5 mm is associated with a normalized thallium uptake of $>$50%, indicating residual viability (14).

MRI has also been used to define viable myocardium in a region of akinesis by documenting functional reserve during pharmacologic stress (15). Similar to stress echocardiography, MRI can be used to predict viability by demonstrating residual contractile response to inotropic drugs by providing precise measurement of wall thickening (16,17) (Fig. 1). Using 18-fluorodesoxyglucose PET as a reference standard to define viability in patients with chronic myocardial infarctions, Baer et al. (18) compared dobutamine transesophageal echocardiography with dobutamine cine MRI. They found that the sensitivities of stress transesophageal echocardiography and cine MRI for PET-defined viability were 77% versus 81%, whereas specificities were 94% versus 100%. In another study (19), the same investigators demonstrated that a preserved diastolic wall thickness $\geq$5.5 mm and dobutamine-induced systolic wall thickening $\geq$1 mm characterized viable myocardium as defined by PET. Moreover, dobutamine-induced systolic wall thickening of $\geq$2 mm was found to be a better predictor of regional functional recovery after revascularization (sensitivity, 89%, and specificity, 94%) than preserved diastolic wall thickening (sensitivity, 92%, and specificity, 56%) (20). On the other hand, a significantly reduced diastolic wall thickening $<$5.5 mm was a reliable indicator of irreversible myocardial damage (20). Compared with pooled data from nu-

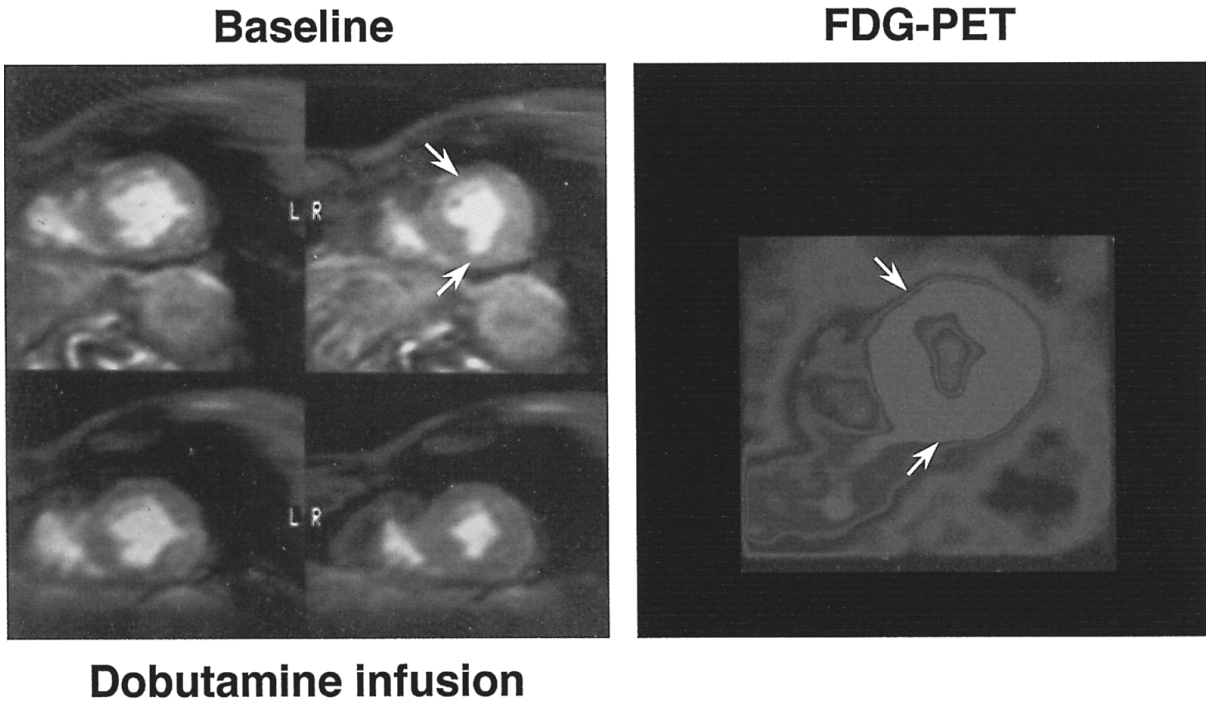

Figure 1. (Left) Short-axis cine MR (GRE) images (TR/TE 28/12) at baseline (top) and during low-dose dobutamine infusion (bottom) in a patient with chronic anteroseptal and inferior infarction. Wall thinning on the end-diastolic image (top left) and absent regional wall thickening on the end-systolic image indicated by black arrows (top right) is seen at baseline. During low-dose dobutamine stimulation (10 μg/kg/min), marked improvement of wall thickening and wall motion is noted (diastole, lower left; systole, lower right). (Right) Corresponding PET image shows preserved fluorodesoxyglucose uptake indicating residual viability in infarcted areas marked by white arrows. (Courtesy of Dr. Udo Sechtem, Robert-Bosch-Krankenhaus, Stuttgart, Germany.) (From Ref. 16.)

clear studies (21), MRI-measured wall thickening with pharmacologic stress appears to have a higher accuracy in predicting functional recovery after successful revascularization (Table 1). Using dobutamine cine MRI to predict functional improvement in patients with recent myocardial infarctions was also shown to be feasible (22,23).

Monitoring ventricular wall motion by MR tagging provides additional information on the effects of ischemia and infarction on regional function. Myocardial tagging was introduced first by Zerhouni et al. (24) in the late 1980s, and several alternative tagging schemes have been developed since (25). The basis of all tagging schemes is similar. The magnetization of specific regions of myocardium is modulated at a given time point in the cardiac cycle and then the displacement of the tagged regions is tracked over a series of images. Using this technique, the motion of myocardium can be followed noninvasively in three-dimensional space, and wall motion parameters, such as regional shortening, strain, and torsion, can be assessed quantitatively. Animal models of myocardial infarction showed that the extent of dysfunctional myocardium far exceeds the extent of necrosis. Not only stunned adjacent myocardium but also remote normally perfused tissue exhibited abnormal deformation patterns as demonstrated with myocardial tagging (26,27).

The combination of pharmacologic stress with myocardial tagging provides further insights for the differentiation between viable and nonviable myocardium (23,28,29). Moreover, MR tagging enables transmural resolution of response to inotropic stimulation and can display differences in subendocardial, mid, and subepicardial layers. In this regard, Geskin et al. (23) evaluated 20 patients with reperfused myocardial infarctions with tagged MRI at rest and during dobutamine stress in the first week after infarction. A normal dobutamine-elicited increase in circumferential segment shortening within dysfunctional mid-ventricular and subepicardial layers

Table 1

Sensitivity and Specificity for Different Imaging Techniques in Predicting the Gold Standard of Functional Recovery After Successful Revascularization

Reference Number	Imaging Technique	No. of Patients	Sensitivity (%)	Specificity (%)
21	^{18}FDG PET	332	88	73
21	Rest-redistribution ^{201}thallium SPECT	145	90	54
21	^{99m}Technetium sestamibi	207	83	69
21	Low dose dobutamine echocardiography	448	84	81
20	MRI-preserved DWT (≥5.5 mm)	43	92	56
20	MRI dobutamine–induced SWT (≥2mm)	43	89	94
28	Stress MRI with tagging	10	89	93
53	Contrast-enhanced MRI—lack of delayed hyperenhancement	12	98	76

Reference 21 represents data from a pooled analysis.
DWT, diastolic wall thickness; SWT, systolic wall thickening; ^{18}FDG, fluorodeoxyglucose.

was predictive of functional recovery at 8 weeks after infarction. However, the response within the subendocardium was not predictive of return of function.

The potential advantage of cine MRI over echocardiography is quantification of the extent and severity of wall motion abnormalities along with consistent image quality independent of an acoustic window. However, several limitations apply to the MR approach: 1) lack of portability; 2) problem with electrocardiographic gating, especially in patients with arrhythmias; 3) need to control for cardiac and respiratory motion; 4) limited monitoring and access in case of the emergency situation; and 5) complex analysis of MR images, especially tagged MRI.

TISSUE CHARACTERIZATION

Unenhanced T2-Weighted MR Images

Several studies have shown that acute and subacute myocardial infarction can be detected as a bright region on unenhanced T2-weighted SE images (30,31). These changes are most likely due to edema in the ischemically injured region. It has been shown that the size of the bright region and the intensity of the signal diminish over time (32). Early after the infarct, T2-weighted images tend to overestimate the area of necrosis (30,33), whereas after 3 weeks a good correlation exists between true infarct size and the area of hyperintensity (32). More recent research has confirmed these findings. Choi et al. (34) also reported an overestimation of the infarction size using a breathhold T2-weighted imaging sequence. By comparing with electron microscopy, they concluded that T2-weighted images include the infarcted and the periinfarcted area.

Contrast-Enhanced MRI

In recent years, MR contrast media have been applied using several unique strategies for the characterization of ischemic heart disease and the assessment of myocardial viability (35,36). These include the use of dynamic imaging to assess tissue perfusion and to identify regions with abnormal wash-in/wash-out profiles, extravascular contrast agents to probe cellular membrane integrity, necrosis-specific contrast media to highlight the zone of irreversible injury, and slow-release manganese agents to probe ionic transport across functional cell membranes.

Dynamic Imaging

Fast MRI techniques made it possible to monitor the passage of contrast medium through the heart (37) and to detect differences in enhancement between normally perfused myocardium and the area of jeopardy supplied by a coronary artery with significant stenosis (38,39) (Fig. 2). Dipyridamole-stress MRI enhances the detection of hypoperfused myocardium in the presence of critical coronary stenosis during the first pass of MR contrast media (40). Moreover, it has been shown that first-pass contrast-enhanced sequences can be quantified for estimating regional myocardial blood flow and volume (41).

In a rat model of reperfused myocardial infarction, Saeed et al. (42) demonstrated that enhancement of irreversibly injured myocardium after contrast administra-

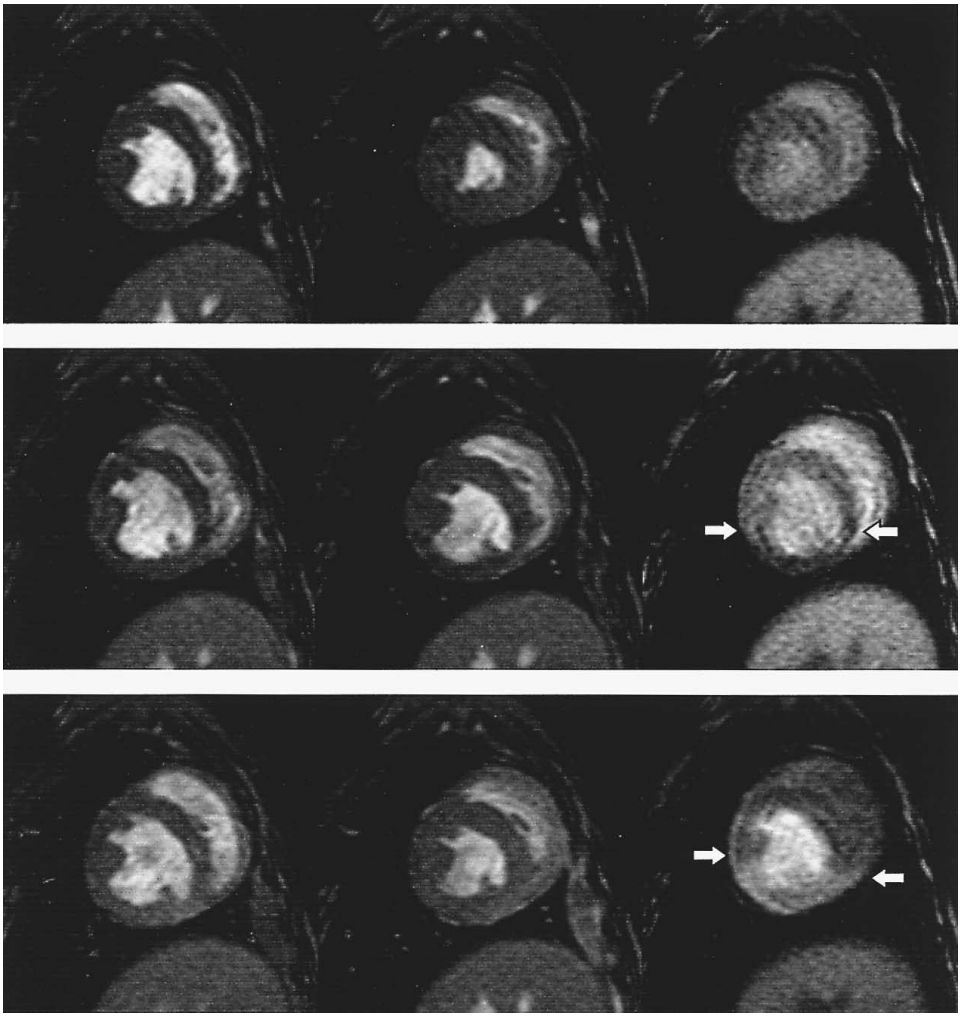

Figure 2. Combined functional and perfusion MRI of a canine heart at (top) baseline, (middle) during circumflex coronary artery occlusion, and (bottom) within 5 min after reperfusion. In each row, the left and middle images show short-axis images at end-diastole and end-systole using breathhold segmented fast GRE (TR/TE 6.9/2.3) for wall thickness measurements; the right image shows diastolic images obtained during peak enhancement of bolus injection of Gd-DTPA-BMA using inversion-recovery fast GRE (TR/TI/TE 6.9/700/2.3) to monitor first pass of the agent. During occlusion (middle), the posterior wall shows impaired contractility and the ischemic zone is shown as a dark area ''cold spot'' (arrows). During reperfusion (bottom), the same zone appears as a bright area (arrows) and wall thickening improves but remains diminished compared with baseline. (From Ref. 39.)

tion was delayed but increased steadily to a higher level than normal myocardium. This study, using a methodology with high temporal resolution, demonstrated that the enhancement kinetics of irreversibly injured reperfused myocardium is not identical to reversibly injured or normal myocardium.

Using a magnetization-driven GRE imaging sequence, Lima et al. (43) observed two different distribution patterns of MR contrast media in patients with reperfused myocardial infarctions during the first 10 min after bolus administration. In 21 patients they found hyperenhancement within the infarcted region. However, in 10 of these patients, this hyperenhanced region surrounded a subendocardial area of decreased signal intensity, which diminished in size over the course of 5–8 min after bolus administration. This pattern was associated with occluded or severely stenotic infarct-related arteries at the time of cardiac catheterization, the presence of Q waves on the electrocardiogram, and greater segmental dysfunction by echocardiography. The investigators hypothesized that

this phenomenon was caused by severe capillary damage and/or microvascular obstruction at the core of the infarcted region.

These clinical observations have been confirmed by experimental findings using a similar imaging sequence (44–47). In a canine model of 2-day-old reperfused infarctions, Judd et al. (44) observed the same enhancement pattern on postcontrast MR images. As suggested in the patient study, subendocardial zones of hypoenhancement on first-pass images (0–2 min after bolus administration) matched closely with those of thioflavin-negative regions, indicating no reflow. Surrounding zones of hyperenhancement on delayed images (obtained 6–14 min after contrast injection) correlated with necrotic myocardium defined by triphenyltetrazolium chloride (TTC) histochemical staining but tended to overestimate the area of infarction by 12%. Another study with a similar experimental design investigated the progression of the no-reflow zone and infarction size over the course of 48 hr after reperfusion (46). Using contrast-enhanced MRI, the authors demonstrated that the extent of microvascular obstruction and the infarction size increased over the first 48 hr after myocardial infarction. Similar to the previous study (44), the hyperenhanced zone correlated well with infarct size measured by TTC on postmortem examination but overestimated it by 9.4%. By comparing ex vivo T1-weighted three-dimensional GRE images with TTC staining, it was also reported (48) that the spatial extent of hyperenhancement in acute and chronic infarcts was identical to that of myocyte necrosis or scar tissue in a dog model of myocardial injury. They stated that partial volume effects might have contributed to the overestimation of infarct size in their previous studies.

Further clinical studies explored the temporal pattern of myocardial contrast enhancement to predict myocardial viability in acute reperfused myocardial infarctions (49–51). Rogers et al. (49) examined 17 patients at 1 and 7 weeks after reperfusion by MR tagging to evaluate contractile function and at 1 week by T1-weighted inversion recovery turbo fast low-angle shot sequence (FLASH) images to monitor first-pass and delayed enhancement up to 7 ± 2 min after contrast administration. All patients had normal flow (thrombolysis in myocardial infarction grade 3) in the infarct-related artery. Three distinct patterns of abnormal enhancement were observed in injured areas: hypoenhancement during first pass without delayed enhancement (HYPO), normal first-pass signal followed by hyperenhancement on delayed images (HYPER), and hypoenhancement on first-pass and delayed hyperenhancement (COMB). Regions characterized as HYPER exhibited significant improvement in function after 7 weeks, signifying viability, whereas HYPO regions did not improve and COMB regions showed borderline improvement (Table 2). In another study (50), they observed similar contrast enhancement patterns in 19 patients with 3 ± 1-day-old infarctions. Using T1-weighted SE imaging, Dendale et al. (51) related contrast enhancement patterns on delayed images to viability defined by inotropic response during dobutamine stress MRI in patients with less than 2-week-old infarctions. They reported that absent or only subendocardial hyperenhancement was related to functional recovery under stress in 83% (31/37) of infarct segments. On the other hand, transmural hyperenhancement corresponded to no contractile reserve in 59% (10/17) of infarct segments but corresponded to normally functioning segments or segments with responsiveness to dobutamine in 41% (7/17), indicating residual viability in almost half of the segments with transmural enhancement. Overall, the results of these clinical studies (49–51) point out that the combined assessment of first-pass and delayed imaging may predict viability, whereas the assessment of delayed hyperenhancement itself leads to low specificity for the determination of viability in patients with acute reperfused myocardial infarction.

Table 2

Abnormal Contrast Enhancement Patterns in Injured Areas and Their Functional Outcome After 7 Weeks in Patients With Acute Reperfused Infarctions

Abnormal Pattern	First-Pass Hypoenhancement	Delayed Hyperhancement	Shortening Baseline (%)	Shortening Follow-up (%)	Functional Outcome After 7 Weeks
HYPO	+	−	5 ± 4	6 ± 3	No improvement (p = ns)
COMB	+	+	7 ± 6	11 ± 5	Borderline improvment ($p = 0.06$)
HYPER	−	+	9 ± 8	18 ± 5	Improvement ($p < 0.001$)

From Ref. 49.

Two studies investigated the role of hyperenhancement in patients with subacute or chronic myocardial infarctions (52,53). Using a magnetization-driven GRE imaging sequence, Ramani et al. (52) tested the feasibility of contrast MRI to assess viability in patients with stable coronary artery disease and LV dysfunction and compared the MR findings with rest-redistribution ^{201}Tl imaging. In this study, 22 of 24 patients had a history of myocardial infarction and in most of them the infarction occurred >6 months before entering the study. The authors found that the combination of contraction pattern and delayed contrast enhancement further improved the accuracy to predict viability. For example, the presence of delayed hyperenhancement correlated most closely with nonviability in segments that were akinetic or dyskinetic under resting conditions (83% concordance). However, in segments with resting hypokinesis, 58% of segments showing hyperenhancement were judged viable by ^{201}Tl SPECT. Therefore, the authors concluded that these segments may have represented an admixture of scar tissue and viable myocardium. However, it should be noted that rest redistribution ^{201}Tl imaging has an average specificity of 54% in relation to the gold standard of improved contractile function after revascularization and may therefore overestimate the presence of viable myocardium (21). Sandstede et al. (53) examined 12 patients with regional wall motion abnormalities (10 with a history of previous infarction 27 ± 9 days before the examination) with MRI before and after revascularization. Using a T1-weighted inversion recovery turbo-FLASH sequence, they acquired first-pass and delayed images at 15 min after injection of gadolinium chelate. Improved systolic wall thickening after revascularization served as criterion of viability. Three months after revascularization, 25 of 26 hyperenhanced segments (96%) did not recover function, whereas 39 of 47 segments without hyperenhancement (83%) showed functional improvement. The authors concluded that segments with delayed enhancement are nonviable (Table 1). However, it should be noted that with one exemption, all segments with delayed hyperenhancement exhibited hypoenhancement during first pass. Referring to the nomenclature of Rogers et al. (49), this pattern represents COMB. The study of Sandstede et al. (53) seems to be at odds with the results of Rogers et al. (49), who found at least borderline improvement in segments with the COMB pattern. The time of imaging after the infarction, the flow in the infarct-related artery, the dosages of contrast media, and differences in the assessment of functional recovery (with or without tagging) may have contributed to this conflicting findings in these two studies.

From several studies it can be concluded that the presence of hypoenhancement on either first-pass or delayed images is predictive of nonviability and regional dysfunction (43,44,47,49–51,54) . However, it should be noted that hypoenhanced myocardium represents an area of no reflow within the injured region and therefore underestimates the true infarction size. Perfusion MR and contrast echocardiography studies (54,55) also showed that no reflow at the tissue level despite patency of the infarct-related vessel is a strong predictor of poor functional recovery and more frequent cardiovascular complications.

The role of hyperenhancement on delayed images (Fig. 3) is less clear and still controversial. Earlier experimental work from Judd et al. (44) indicated that hyperenhanced myocardium closely correlates but overestimates the true infarction size measured by TTC. In a more recent study, Kim et al. (48) indicated that hyperenhanced myocardium matches exactly with area of necrosis or scar tissue. Other groups (34,56–60) found that areas of hyperenhancement overestimate the extent of acute myocardial infarction and represent a mixture of viable rim and nonviable core. This is in line with results from human studies that suggest viable myocardium may be found within hyperenhanced, but not hypoenhanced, regions (49–51). However, the following factors should be considered in defining viability or nonviability from contrast enhanced regions: age of infarct, flow in the infarct-related artery, type of imaging sequence and its sensitivity to T1 changes,dosage of contrast media and time of

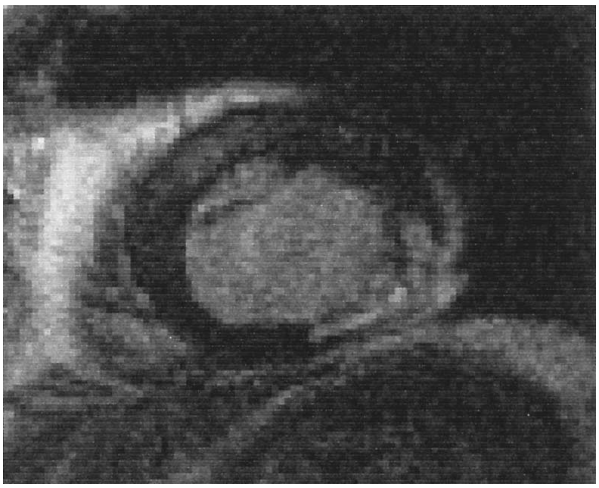

Figure 3. End-diastolic, short-axis, T1-weighted, inversion recovery, turbo-FLASH image (TR/TI/TE 400/300/4) obtained 15 min after administration of 0.1 mmol/kg Gd-DTPA in a patient with 4-month-old posterior myocardial infarction. Note the late hyperenhancement in the posterior-lateral wall.

imaging after contrast administration, slice thickness and partial volume effects, and the ''reference standard'' used to infer viability. Further research is needed to resolve this issue.

Detection of Myocyte Membrane Damage

With this approach, myocardial viability is determined by estimating the breakdown of cellular membranes within a zone of ischemic injury using nonspecific extravascular contrast media. These agents can increase or decrease signal intensity depending on the type and the concentration of contrast media in the tissue and the MR sequence used. Relaxivity- or T1-enhancing contrast media, such as Gd-DTPA, usually increase MR signal in tissue not excluded from blood supply on T1-weighted images, whereas susceptibility- or T2*-enhancing agents, such as dysprosium-DTPA, cause a signal loss with T2-sensitive imaging sequences. These two types of contrast media freely exit from the vascular space and rapidly distribute in the extracellular space but are excluded from the intracellular compartment of cells with intact membranes.

After administration of dysprosium-DTPA, signal attenuation is a function of magnetic susceptibility and distribution within the tissue with a greater effect associated with more heterogeneous distribution. In normal myocardium, cell membranes act as a barrier and limit the distribution of contrast agent to the extracellular space, causing heterogeneous distribution in tissue with attenuation of signal. Reperfused myocardial infarctions in a rat model displayed less signal attenuation than normal myocardium after the administration of dysprosium-DTPA (61). It was concluded that this effect was the result of a more homogeneous distribution of dysprosium in the infarcted myocardium, which is consistent with the breakdown of cell membranes and contrast agent entering the intracellular space. A subsequent study corroborated this finding and supported the proposed mechanism (62). Chemical measurements in excised hearts showed a 2.5-fold higher tissue content of dysprosium-DTPA in reperfused infarcted myocardium compared with normal myocardium despite the higher signal of the infarcted myocardium due to attenuation of the effect of dysprosium (62). It was concluded that the loss of magnetic susceptibility effect exerted by dysprosium-DTPA was caused by the failure of myocardial cells to exclude the compound instead of a reduced tissue concentration.

The relative content of Gd-DTPA in myocardium and blood during a near equilibrium state after intravenous administration (3–30 min) and hence its effect on T1-shortening ($\Delta R1$) and signal intensity can be expressed as the relative fractional distribution volume. In myocardium, it can be calculated from the product of the ratio of $\Delta R1$ myocardium/$\Delta R1$ blood with the fractional distribution volume in the blood expressed by the formula $\Delta R1myo/\Delta R1blood \times (1 - \text{hemotocrit})$. With the loss of cellular membrane integrity, there is no barrier between extracellular and intracellular compartments; consequently, the fractional distribution volume of gadolinium is expanded from approximately 20% in normal myocardium up to nearly 100% in complete myocardial necrosis. As the distribution volume increases, the bulk tissue concentration of extracellular contrast agents also increases.

Pereira et al. (63) demonstrated that indirect measurement of the tissue content of Gd-DTPA in excised hearts of reperfused infarctions was inversely related to myocardial viability assessed by ^{201}Tl uptake. In a follow-up study, these authors showed that in vivo measurement of the partition coefficient (λ), which is proportional to the fractional distribution volume, agreed well with values determined ex vivo from radioactive counting of ^{111}In-DTPA. Furthermore, MRI allowed monitoring of these values over time as early as 1 min and up to 8 weeks after reperfusion of acute myocardial infarction (64).

Wendland et al. (65) used an inversion recovery echo planar technique to follow the change in T1 relaxation rate ($\Delta R1$), which is proportional to the quantity of contrast medium within the tissue of interest, over the course of time after administration of gadolinium chelates. They found a constant proportionality between $\Delta R1$ ratio of myocardial tissue and the blood pool during the first 30 min after injection of gadolinium chelates and a failure of increased doses of the agent to alter this proportionality consistent with the concept of near equilibrium state of distribution. Subsequently, these investigators used this approach to estimate the distribution volume of gadolinium chelates in normal and ischemically injured myocardium (66). They also compared the fractional distribution volume of Gd chelates with ^{99m}Tc-DTPA autoradiography as an independent reference (57,66,67). The distribution volumes measured by MRI and autoradiography were almost identical, and in complete infarction a distribution volume of 90% of tissue space indicated entrance of the indicators into nearly all myocardial cells. In an animal model of graded myocardial injury, they showed that the distribution volume of Gd-DTPA-BMA increased in relation to the duration of coronary occlusion (57,66) (Fig. 4). They also demonstrated that postischemic myocardium exhibited two regions of abnormally elevated count density at autoradiography: a core of high count density surrounded by a rim of moderate count den-

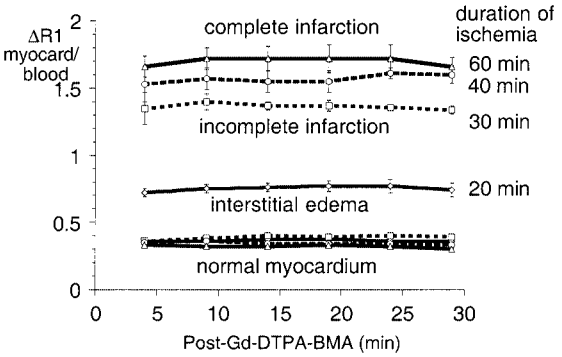

Figure 4. Plot of the effect of duration of ischemia on ΔR1 ratio in rats subjected to 20, 30, 40, and 60 min of coronary occlusion followed by 1 hr of reperfusion. During repetitive measurements, the ΔR1 ratios for myocardium/blood remain constant during the initial 30 min after contrast injection of Gd-DTPA-BMA, suggesting a near equilibrium state. This means that ΔR1 ratios represent partition coefficients (λ), which allows calculation of fractional distribution volume. Note the increase in ΔR1 ratio as a function of the severity of injury.

sity (57). The distribution volume of Gd-DTPA-BMA and its surrogate ^{99m}Tc-DTPA in the rim was approximately twofold larger than that of normal myocardium (20%) but half that of the infarct core (>80%). By electron microscopy they showed that the rim contained moderately injured myocardium comprised largely of viable cells. Therefore, the authors concluded that this method provides an estimate of the percentage of necrotic cells within a zone of injury.

In summary, quantifying the distribution volumes rather than visually identifying regions of hyperenhancement after administration of Gd-DTPA might provide additional information for determining myocardial viability.

Necrosis-Avid Contrast Agents

There have been several efforts in the past to devise a contrast agent that selectively binds to regions of infarcted myocardium. Notable attempts include binding an indicator to antibodies specific for intracellular compounds (68) or using phosphonate-modified gadolinium chelates that interact with calcium deposits that accumulate in necrotic tissue (69).

More recently, the necrosis-avid property of porphyrin-based compounds was described and tested in animal models of acute myocardial infarctions (70,71). Due to the well-known affinity of porphyrins for tumors, metalloporphyrins were investigated initially as tumor-seeking MRI contrast media. However, the discovery of a more necrosis-specific rather than a tumor-specific property of one such agents (gadolinium mesoporphyrin or gadophrin-2) changed the whole scenario. Ni, Marchal, and their colleagues (70,71) were the first to use this agent to visualize myocardial necrosis in animals with occlusive and reperfused myocardial infarctions. They found a sharp demarcation (hyperenhancement) of the infarcted area on T1-weighted SE images after intravenous injection of gadophrin-2 that matched in detail with the histomorphologic area of myocardial necrosis defined by TTC staining. In a follow-up study, Pislaru et al. (72) induced coronary artery thrombosis in dogs, followed by thrombolytic therapy after 90 min of occlusion. MRI was performed in vivo and in vitro 24 hr after administration of gadophrin-2. Again the hyperenhanced area on gadophrin-2–enhanced T1-weighted images precisely demarcated the infarct size compared with the reference standard TTC staining.

Saeed et al. (56) induced reversible and irreversible myocardial injury in rats and administered a nonspecific T1-shortening agent, Gd-DTPA, and a necrosis-specific compound, gadophrin-2, at different time points after reperfusion. In animals with irreversibly injured myocardium, the size of the gadophrin-2–enhanced regions closely matched the size of infarction defined by TTC. Using T1-weighted SE imaging, the enhanced region by Gd-DTPA (29 min after contrast administration) overestimated the size of the true infarction but was close to the area at risk defined by phthalocyanine blue dye injection after reocclusion of the coronary artery. The authors concluded that the difference in size demarcated by the two compounds may provide an estimation of injured but viable myocardium. In another study, Saeed et al. (60) corroborated these findings. Using functional and contrast-enhanced MRI with necrosis-specific and standard extracellular contrast media, the authors could demonstrate that 24 hr after reperfusion the Gd-DTPA enhanced zone encompasses viable and nonviable portions (Fig. 5).

Ion Transport Contrast Media

Like gadolinium, manganese-based compounds are also strongly paramagnetic contrast media. So far, Mn-DPDP is approved in humans for clinical hepatic imaging at a dose of 5 μmol/kg. This contrast agent was also explored for myocardial imaging 10 years ago using a high dose of 400 μmol/kg (73). In the meantime, it was reported that the manganese cation is slowly released from the chelate (74) and quickly taken up via voltage operated calcium channels and retained in viable myocardial cells

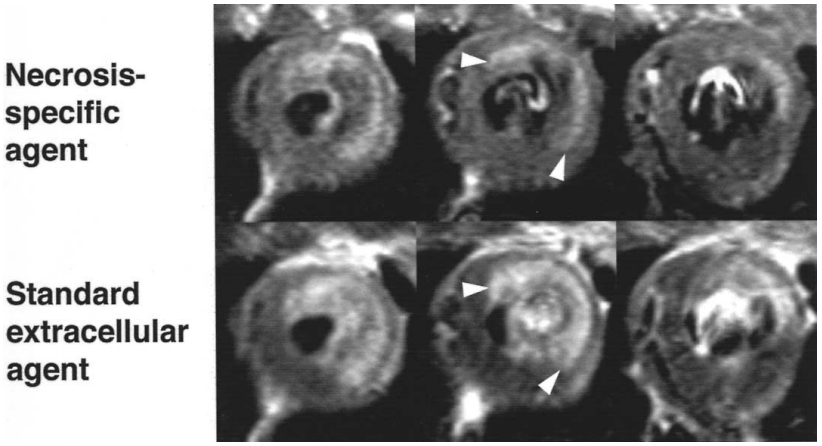

Figure 5. Short-axis, T1-weighted, SE images (TR/TE 300/12) at the level of apex (left), center (middle), and base (right) of the left ventricle in a rat heart subjected to reperfused myocardial injury. Images were obtained in the same imaging session after the administration of a necrosis-specific agent, gadophrin-2 (top), followed by a standard extracellular contrast medium, Gd-DTPA (bottom), 24 hr after reperfusion. Note that the size of the hyperenhanced zone on Gd-DTPA enhanced images is substantially larger than that on gadophrin-2 enhanced images. This difference between the hyperenhanced zone may represent salvageable peri-infarcted myocardium.

for hours (75,76). Therefore, it might be possible to obtain post–Mn-DPDP MR images in which contrast is primarily provided by the uptake of manganese released from the chelate. A recent study (77) demonstrated the accumulation of manganese in normal myocardium and rapid clearance from infarcted myocardium during a 1-hr period after administration of several doses of Mn-DPDP (25, 50, and 100 μmol/kg) in an animal model (Fig. 6). These results suggest that manganese compounds might be useful to assess myocardial viability with MRI, because only viable cells are able to retain this contrast media.

CONCLUSION

MR techniques for viability are intriguing and will be competitive with echocardiography and radionuclide imaging in the near future. Even though several MR approaches to define myocardial viability have been shown

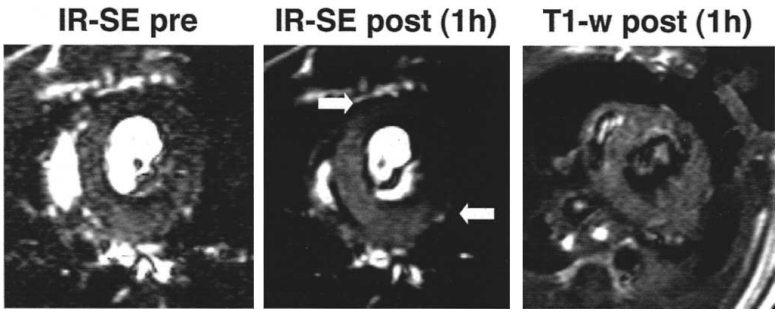

Figure 6. Short-axis inversion recovery SE (TR/TI/TE 1000/500/12) and conventional T1-weighted SE (TR/TE 300/12) images acquired precontrast (left) and postcontrast injection of 100 μmol/kg Mn-DPDP (middle and right) at the mid-ventricular level. Note the dark appearance of the infarcted zone (arrows) 1 hr postinjection using inversion recovery SE imaging, whereas normal myocardium appears bright due to uptake of paramagnetic Mn^{2+} ions. The nonviable zone is not visualized on unenhanced inversion recovery SE images and enhanced conventional T1-weighted SE images.

to be feasible, the usage of MR in ischemic heart disease is still limited compared with the ubiquity and widespread acceptance of echocardiography and radionuclide imaging. However, the ongoing progress and the variety of potential MR methods for achieving this goal are promising. Nevertheless, MR can contribute to the assessment of patients with coronary heart disease in a number of different ways. The coupling of noninvasive coronary angiography and coronary flow measurements should move MRI into a prominent position in the diagnosis and management of coronary heart disease in the near future. By providing all this information, MRI may become more cost effective than other imaging modalities.

ACKNOWLEDGMENTS

N. W. is supported by a Postdoctoral Research Exchange Grant from the Max-Kade Foundation, Inc., New York.

REFERENCES

1. Rahimtoola, S.H. The Hibernating Myocardium. Am. Heart. J. **1989**, *117*, 211–221.
2. Haas, F.; Haehnel, CJ.; Picker, W.; Nekolla, S.; Martinoff, S.; Meisner, H.; Schwaiger, M. Preoperative Positron Emission Tomographic Viability Assessment and Perioperative and Postoperative Risk in Patients With Advanced Ischemic Heart Disease. J. Am. Coll. Cardiol. **1997**, *30*, 1693–1700.
3. Braunwald, E.; Kloner, R.A. The Stunned Myocardium: Prolonged, Postischemic Ventricular Dysfunction. Circulation, **1982**, *66*, 1146–1149.
4. Bolli, R.; Zhu, W.X.; Thornby, J.I.; O'Neill, P.G.; Roberts, R. Time Course and Determinants of Recovery of Function After Reversible Ischemia in Conscious Dogs. Am. J. Physiol. **1988**, *254*, 102–114.
5. Gropler, R.J.; Bergmann, S.R. Myocardial Vability—What Is the Definition? J. Nucl. Med. **1991**, *32*, 10–12.
6. Higgins, C.B. Prediction of Myocardial Viability by MRI. Circulation **1999**, *99*, 727–729.
7. Bax, J.J.; de Roos, A.; van der Wall, E.E. Assessment of Myocardial Viability by MRI. J. Magn. Reson. Imaging **1999**, *10*, 418–422.
8. Mallory, G.K.; White, P.D.; Salcedo-Galger, J. The Speed of Healing of Myocardial Infarction: A Study of Pathologic Anatomy in 72 Cases. Am. Heart J. **1939,** *18*, 647–671.
9. Sechtem, U.; Eberhard, V.; Baer, F.; Schneider, C.; Theissen, P.; Schicha, H. Assessment of Residual Viability in Patients With Myocardial infarction Using Magnetic Resonance Techniques. Int. J. Cardiol. Imaging **1993**, *9*, 31–40.
10. Higgins, C.B.; Lanzer, P.; Stark, D.; Botvinick, E.; Crooks, N.B.; Kaufman, L.; Lipton, M.J. Imaging by Nuclear Magnetic Resonance in Patients With Chronic Ischemic Heart Disease. Circulation **1984**, *69*, 523–531.
11. McNamara, M.T.; Higgins, C.B. Magnetic Resonance Imaging of Chronic Myocardial infarcts in Man. AJR Am. J. Roentgenol. **1986**, *146*, 315–320.
12. Baer, F.M.; Smolarz, K.; Jungeheulsing, M.; Beckwilm, J.; Theissen, P.; Sechtem, U,; Schicha, H.; Hilger, H.H. Chronic Myocardial Infarction, Assessment of Morphology, Function and Perfusion by Gradient Magnetic Resonance Imaging and 99mTC-Methoxyisobutyl-Isonitrile SPECT. Am. Heart J. **1992**, *123*, 636–645.
13. Perrone-Filardi, P.; Bacharach, S.L.; Dilsizian, V.; Maurea, S.; Frank, J.A.; Bonow, R.O. Regional Left Ventricular Wall Thickening: Relation to Regional Uptake of ^{18}fluorodeoxyglucose and ^{201}Tl in Patients With Chronic Coronary Artery Disease and Left Ventricular Dysfunction. Circulation **1992**, *86*, 1125–1137.
14. Lawson, M.A.; Johnson, L.L.; Coghlan, L.; Alami, M.; Tauxe, E.L.; Reinert, S.E.; Singleton, R.; Pohost, G.M. Correlation of Thallium Uptake With Left Ventricular Wall Thickness by Cine Magnetic Resonance Imaging in Patients With Acute and Healed Myocardial Infarcts. Am. J. Cardiol. **1997**, *80*, 434–441.
15. Pennel, D.J.; Underwood, S.R. Stress Cardiac Magnetic Resonance Imaging. Am. J. Cardiol. Imaging **1991**, *5*, 139–149.
16. Sechtem, U.; Baer, F.M.; Voth, E.; Theissen, P.; Schneider, C.A. Stress Functional MRI: Detection of Ischemic Heart Disease and Myocardial Viability. J. Magn. Reson. Imaging **1999**, *10*, 667–675.
17. Dendale, P.A.C.; Franken, P.R.; Waldman, G.J.; De Moor, D.G.; Tombeur, D.A.; Block, P.F.; De Roos, A. Low-Dosage Dobutamine Magnetic Resonance Imaging as an Alternative to Echocardiography in the Detection of Viable Myocardium After Acute Infarction. Am. Heart J. **1995**, *130*, 134–140.
18. Baer, F.M.; Voth, E.; Larosèe, K.; Schneider, C.A.; Theissen, P.; Schicha, H.; Sechtem, U. Comparison of Dobutamine Transesophageal Echocardiography and Dobutamine Magnetic Resonance Imaging for Detection of Residual Myocardial Viability. Am. J. Cardiol. **1996**, *78*, 415–419.
19. Baer, F.M.; Voth, E.; Schneider, C.A.; Theissen, P.; Schicha, H.; Sechtem, U. Comparison of Low-Dose Dobutamine-Gradient Echo Magnetic Resonance Imaging and Positron Emission Tomography With [18]Fluorodesoxyglucose in Patients With Chronic Coronary Artery Disease: A Functional and Morphological Approach to the Detection of Residual Myocardial Viability. Circulation **1995**, *91*, 1006–1015.
20. Baer, F.M.; Theissen, P.; Schneider, C.A.; Voth, E.; Sechtem, U.; Schicha, H.; Erdmann, E. Dobutamine Mag-

netic Resonance Imaging Predicts Contractile Recovery of Chronically Dysfunctional Myocardium After Successful Revascularization. J. Am. Coll. Cardiol. **1998**, *31*, 1040–1048.
21. Bax JJ.; Wijns W.; Cornel JH.; Visser FC.; Boersma, E.; Fioretti PM. Accuracy of Currently Available Techniques For Prediction of Functional Recovery After Revascularization in Patients With Left Ventricular Dysfunction Due to Chronic Coronary Artery Disease: Comparison of Pooled Data. J. Am Coll. Cardiol. **1997**, 30, 1451–1060.
22. Dendale, P.; Franken, P.R.; Holman, E.; Avenarius, J.; Van Der Wall, E.E.; De Roos, A. Validation of Low-Dose Dobutamine Magnetic Resonance Imaging for Assessment of Myocardial Viability After Infarction by Serial Imaging. Am. J. Cardiol. **1998**, *82*, 375–377.
23. Geskin, G.; Kramer, C.M.; Rogers, W.J.; Theobald, T.M.; Pakstis, D.; Hu, Y.L.; Reichek, N. Quantitative Assessment of Myocardial Viability After Infarction by Dobutamine Magnetic Resonance Tagging. Circulation **1998**, *98*, 217–223.
24. Zerhouni, E.A.; Parish, D.M.; Rogers, W.J.; Yang, A.; Shapiro, E.P. Human Heart: Tagging With MR Imaging—A Method for Noninvasive Assessment of Myocardial Motion. Radiology **1988**, *169*, 59–63.
25. Axel, L.; Dougherty, L. MR Imaging of Motion With Spatial Modulation of Magnetization. Radiology **1989**, *171*, 841–845.
26. Kramer, C.M.; Lima, J.A.C.; Reichek, N.; Ferrari, V.A.; Ilaneras, M.R.; Palmon, L.C.; Yeh, I.T.; Tallant, B.; Axel, L. Regional Differences in Function Within Noninfarcted Myocardium During Left Ventricular Remodeling. Circulation **1993**, *88*, 1279–1288.
27. Kraitchman, D.L.; Young, A.A.; Bloomgarden, D.C.; Fayad, Z.A.; Dougherty, L.; Ferrari, V.A.; Boston, R.C.; Axel, L. Integrated MRI Assessment of Regional Function and Perfusion in Canine Myocardial Infarction. Magn. Reson. Med. **1998**, *40*, 311–320.
28. Sayad, D.E.; Willett, D.L.; Hundley, W.G.; Grayburn, P.A.; Peshock, R.M. Dobutamine Magnetic Resonance Imaging With Myocardial Tagging Quantitatively Predicts Improvement in Regional Function After Revascularization. Am. J. Cardiol. **1998**, *82*, 1149–1151.
29. Croisille, P.; Moore, C.C.; Judd, R.M.; Lima, J.A.; Arai, M.; McVeigh, E.R.; Becker, L.C.; Zerhouni, E.A. Differentiation of Viable and Nonviable Myocardium by the Use of Three-Dimensional Tagged MRI in 2-Day-Old Reperfused Canine Infarcts. Circulation **1999**, *99*, 284–291.
30. Bouchard, A.; Reeves, R.C.; Cranney, G.; Bishop, S.P.; Pohost, G.M. Assessment of Myocardial Infarct Size by Means of T_2-Weighted ^{1}H Nuclear Magnetic Resonance Imaging. Am. Heart J. **1989**, *117*, 281–289.
31. Dulce, M.C.; Duerinckx, A.J.; Hartiala, J.; Caputo, G.R.; O'Sullivan, M.; Cheitlin, M.D.; Higgins, C.B. MR Imaging of the Myocardium Using Nonionic Contrast Medium, Signal-intensity Changes in Patients With Subacute Myocardial Infarction. AJR Am. J. Roentgenol., **1993**, *160*, 963–970.
32. Wisenberg, G.; Prato, F.S.; Carroll, S.E.; Turner, K.L.; Marshall, T. Serial Nuclear Magnetic Resonance Imaging of Acute Myocardial Infarction With and Without Reperfusion. Am. Heart J. **1988**, *115*, 510–518.
33. Ryan, T.; Tarver, R.D.; Duerk, J.L.; Sawada, S.G.; Hollenkamp, N.C. Distinguishing Viable From Infarcted Myocardium After Experimental Ischemia and Reperfusion by Using Nuclear Magnetic Resonance Imaging. J. Am. Coll. Cardiol. **1990**, *15*, 1355–1364.
34. Choi, S.I.; Jiang, C.Z.; Lim, K.H.; Kim, S.T.; Lim, C.H.; Gong, G.Y.; Lim, T.H. Application of Breath-Hold T2-Weighted, First-Pass Perfusion and Gadolinium-Enhanced T1-Weighted MR Imaging for Assessment of Myocardial Viability in A Pig Model. J. Magn. Reson. Imaging **2000**, *11*, 476–480.
35. Wendland, M.F.; Saeed, M.; Lund, G.; Higgins, C.B. Contrast-Enhanced MRI for Quantification of Myocardial Viability. J. Magn. Reson. Imaging **1999**, *10*, 694–702.
36. Saeed, M.; Wendland, M.F.; Higgins, C.B. Contrast Media for MR Imaging of the Heart. J. Magn. Reson. Imaging **1994**, *4*, 269–279.
37. Atkinson, D.J.; Burstein, D.; Edelman, R.R. First-Pass Cardiac Perfusion: Evaluation With Ultrafast MR Imaging. Radiology **1990**, *174*, 757–762.
38. Manning, W.J.; Atkinson, D.J.; Grossmann, W.; Paulin, S.; Edelman, R.R. First-Pass Nuclear Magnetic Resonance Imaging Studies Using Gadolinium-DTPA in Patients With Coronary Artery Disease. J. Am. Coll. Cardiol. **1991**, *18*, 959–965.
39. Szolar, D.H.; Saeed, M.; Wendland, M.F.; Sakuma, H.; Roberts, T.P.; Stiskal, M.A.; Derugin, N.; Higgins, C.B. MR Imaging Characterization of Postischemic Myocardial Dysfunction (''Stunned Myocardium''): Relationship Between Functional and Perfusion Abnormalities. J. Magn. Reson. Imaging **1996**, *6*, 615–624.
40. Saeed, M.; Wendland, M.F.; Sakuma, H.; Geschwind, J.F.; Derugin, N.; Cavagna, F.M.; Higgins, C.B. Coronary Artery Stenosis: Detection With Contrast-Enhanced MR Imaging in Dogs. Radiology **1995**, *196*, 79–84.
41. Wilke, N.; Kroll, K.; Merkle, H.; Wang, Y.; Ishibashi, Y.; Xu, Y.; Zhang, J.; Jerosch-Herold, M.; Mühler, A.; Stillman, A.E. Regional Myocardial Blood Volume and Flow: First-Pass MR Imaging With Polylysine-Gd-DTPA. J. Magn. Reson. Imaging **1995**, *5*, 227–237.
42. Saeed, M.; Wendland, M.F.; Yu, K.K.; Lauerma, K.; Li, H.T.; Derugin, N.; Cavagna, F.M.; Higgins, C.B. Identification of Myocardial Reperfusion With Echo Planar Magnetic Resonance Imaging: Discrimination Between Occlusive and Reperfused Infarctions. Circulation **1994**, *90*, 1492–1501.
43. Lima, J.A.C.; Judd, R.M.; Bazille, A.; Schulman, S.P.; Atalar, E.; Zerhouni, E.A. Regional Heterogeneity of Human Myocardial Infarcts Demonstrated by Contrast-Enhanced MRI: Potential Mechanisms. Circulation **1995**, *92*, 1117–1125.
44. Judd, R.; Lugo-Olivieri, C.H.; Arai, M.; Kondo, T.; Croisille, P.; Lima, J.A.; Mohan, V.; Becker, L.C.; Zerhouni

MARCEL DEKKER, INC.
270 Madison Avenue, New York, New York 10016

E.A. Physiological Basis of Myocardial Contrast Enhancement in Fast Magnetic Resonance Images of 2-Day-Old Reperfused Canine Infarcts. Circulation **1995**, *92*, 1902–1910.

45. Wu, K.C.; Kim, R.J.; Bluemke, D.A.; Rochitte, C.E.; Zerhouni, E.A.; Becker, L.C.; Lima, J.A. Quantification and Time Course of Microvascular Obstruction by Contrast-Enhanced Echocardiography and Magnetic Resonance Imaging Following Acute Myocardial Infarction and Reperfusion. J. Am. Coll. Cardiol. **1998**, *32*, 1756–1764.
46. Rochitte, C.E.; Lima, J.A.C.; Bluemke, D.A.; Reeder, S.B.; McVeigh, E.R.; Furuta, T.; Becker, L.C.; Melin, J.A. Magnitude and Time Course of Microvascular Obstruction and Tissue injury After Acute Myocardial Infarction. Circulation **1998**, *98*, 1006–1014.
47. Gerber, B.L.; Rochitte, C.E.; Melin, J.A.; McVeigh, E.R.; Bluemke, D.A.; Wu, K.C.; Becker, L.C.; Lima, J.A. Microvascular Obstruction and Left Ventricular Remodeling Early After Acute Myocardial Infarction. Circulation **2000**, *101*, 2734–2741.
48. Kim, R.J.; Fieno, D.S.; Parrish, T.B.; Harris, K.; Chen, E.L.; Simonetti, O.; Bundy, J.; Finn, J.P.; Klocke, F.J.; Judd, R.M. Relationship of MRI Delayed Contrast Enhancement to Irreversible injury, Infarct Age, and Contractile Function. Circulation **1999**, *100*, 1992–2002.
49. Rogers, W.J.; Kramer, C.M.; Geskin, G.; HU, Y.L.; Theobald, T.M.; Vido, D.A.; Petruolo, S,; Reichek, N. Early Contrast-Enhanced MRI Predicts Late Functional Recovery After Reperfused Myocardial Infarction. Circulation **1999**, *99*, 744–750.
50. Kramer, C.M.; Rogers, W.J. Jr.; Mankad, S.; Theobald, T.M.; Pakstis, D.L.; Hu, Y.L. Contractile reserve and contrast uptake pattern by magnetic resonance imaging and functional recovery after reperfused myocardial infarction. J. Am. Coll. Cardiol. **2000**, *36*, 1835–1840.
51. Dendale, P.; Franken, P.R.; Block, P.; Pratikakis, Y.; De Roos, A. Contrast Enhanced and Functional Magnetic Resonance Imaging for the Detection of Viable Myocardium After Infarction. Am. Heart J. **1998**, *135*, 875–880.
52. Ramani, K.; Judd, R.M.; Holly, T.A.; Holly, T.B.; Rigolin, V.H.; Parker, M.A.; Callahan, C.; Fitzgerald, S.W.; Bonow, R.O.; Klocke, F.J. Contrast Magnetic Resonance Imaging in the Assessment of Myocardial Viability in Patients With Stable Coronary Artery Disease and Left Ventricular Dysfunction. Circulation **1998**, *98*, 2687–2694.
53. Sandstede, J.J.W.; Lipke, C.; Beer, M.; Harre, K.; Pabst, T.; Kenn, W.; Neubauer, S.; Hahn, D. Analysis of First-Pass and Delayed Contrast-Enhancement Patterns of Dysfunctional Myocardium on MR Imaging: Use in the Prediction of Myocardial Viability. AJR Am. J Roentgenol. **2000**, *174*, 1737–1740.
54. Wu, K.C.; Zerhouni, E.A.; Judd, R.M.; Lugo-Olivieri, C.H.; Barouch, L.A.; Schulman, S.P.; Blumenthal, R.S.; Lima, J.A. Prognostic Significance of Microvascular Obstruction by Magnetic Resonance Imaging in Patients With Acute Myocardial Infarction. Circulation **1998**, *97*, 765–772.
55. Ito, H.; Tomooka, T.; Sakai, N.; Yu, H.; Higashino, Y.; Fujii, K.; Masuyama, T.; Kitabatake, A.; Minamino, T. Lack of Myocardial Perfusion Immediately After Successful Thrombolysis: A Predictor of Poor Recovery of Left Ventricular Function in Anterior Myocardial Infarction. Circulation **1992**, *85*, 1699–1705.
56. Saeed, M.; Bremerich, J.; Wendland, M.F.; Wyttenbach, R.; Weinmann, H.J.; Higgins, C.B. Reperfused Myocardial Infarction as Seen With Use of Necrosis-Specific Versus Standard Extracellular MR Contrast Media in Rats. Radiology **1999**, *213*, 247–257.
57. Arheden, H.; Saeed, M.; Higgins, C.B.; Gao, D.W.; Ursell, P.C.; Bremerich, J.; Wyttenbach, R.; Dae, M.W.; Wendland, M.F. Reperfused Rat Myocardium Subjected to Various Durations of Ischemia: Estimation of the Distribution Volume of Contrast Material With Echo-Planar MR Imaging. Radiology **2000**, *215*, 520–528.
58. Schaefer, S.; Malloy, C.R.; Katz, J.; Parkey, R.W.; Buja, L.M.; Willerson, J.T.; Peshock, R.M. Gadolinium-DTPA-Enhanced Nuclear Magnetic Resonance Imaging of Reperfused Myocardium: Identification of the Myocardial Bed At Risk. J. Am. Coll. Cardiol. **1988**, *12*, 1064–1072.
59. Nishimura, T.; Kobayashi, H.; Ohara, T.; Yamada, N.; Haze, K.; Takamiya, M.; Hiramori, K. Determination of Infarct Size of Acute Myocardial Infarction in Dogs by Magnetic Resonance Imaging and Gadolinium-DTPA: Comparison With Indium-111 Antimyosin Imaging. Am. J. Physiol. **1989**, *4*, 83–88.
60. Saeed, M.; Lund, G.; Wendland, M.F.; Bremerich, J.; Weinmann, H.J.; Higgins, C.B. MR Characterization of the Peri-Infarction Zone of Reperfused Myocardial Infarction Using Necrosis Specific and Extracellular Nonspecific Contrast Media. Circulation **2001**, *103*, 871–876.
61. Saeed, M.; Wendland, M.F.; Masui, T.; Higgins, C.B. Reperfused Myocardial Infarctions on T1- and Susceptibility-Enhanced MRI: Evidence for Loss of Compartmentalization of Contrast Media. Magn. Reson. Med. **1994**, *31*, 31–39.
62. Geschwind, J.F.H.; Wendland, M.F.; Saeed, M.; Lauerma, K.; Derugin, N.; Higgins, C.B. Identification of Myocardial Cell Death in Reperfused Myocardial Injury Using Dual Mechanism of Contrast-Enhanced Magnetic Resonance Imaging. Acad. Radiol. **1994**, *1*, 319–325.
63. Pereira, R.S.; Prato, F.S.; Wisenberg, G.; Sykes, J. The Determination of Myocardial Viability Using Gd-DTPA in a Canine Model of Acute Myocardial Ischemia and Reperfusion. Magn. Reson. Med. **1996**, *36*, 684–693.
64. Pereira, R.S.; Prato, F.S.; Sykes, J.; Wisenberg, G. Assessment of Myocardial Viability Using MRI During a Constant infusion of Gd-DTPA: Further Studies at Early and Late Periods of Reperfusion. Magn. Reson. Med. **1999**, *42*, 60–68.
65. Wendland, M.F.; Saeed, M.; Lauerma, K.; Derugin, N.; Mintorovitch, J.; Cavagna, F.M.; Higgins, C.B. Alterations in T1 of Normal and Reperfused Infarcted Myocardium After Gd-BOPTA Versus Gd-DTPA on Inversion Recovery EPI. Magn. Reson. Med. **1997**, *37*, 448–456.

Marcel Dekker, Inc.
270 Madison Avenue, New York, New York 10016

66. Wendland, M.F.; Saeed, M.; Arheden, H.; Gao, D.W.; Canet, E,; Bremerich, J.; Dae, M.W.; Higgins, C.B. Toward Necrotic Cell Fraction Measurement by Contrast-Enhanced MRI of Reperfused Ischemically injured Myocardium. Acad. Radiol. **1998**, *5*, Suppl. 1, S42–S44.
67. Arheden, H.; Saeed, M.; Higgins, C.B.; Gao, D.W.; Bremerich, J.; Wyttenbach, R.; Dae, M.W.; Wendland, M.F. Measurement of the Distribution Volume of Gadopentetate Dimeglumine at Echo-Planar MR Imaging to Quantify Myocardial Infarction: Comparison With ^{99m}Tc-DTPA Autoradiography in Rats. Radiology **1999**, *211*, 698–708.
68. Weissleder, R.; Lee, A.S.; Khaw, B.A.; Shen, T.; Brady, T.J. Antimyosin-Labelled Monocristalline Iron Oxide Allows Detection of Myocardial Infarct: MR Antibody Imaging. Radiology **1992**, *182*, 381–385.
69. Adzamli, I.K.; Blau, M.; Pfeffer, M.A.; Davis, M.A. Phosphonate-Modified Gd-DTPA Complexes. III: the Detection of Myocardial Infarction by MRI. Magn. Reson. Med. **1993**, *29*, 505–511.
70. Ni, Y.; Marchal, G.; Herijgers, P.; Flameng, W.; Petré, C.; Ebert, W.; Hilger, C.S.; Pfefferer, D.; Semmler, W.; Baert, A.L. Paramagnetic Metalloporphyrins: From Enhancers of Malignant Tumors to Markers of Myocardial Infarcts. Acad. Radiol. **1996**, *3*, Suppl. 2, S395–S397.
71. Marchal, G.; Ni, Y.; Herijgers, P.; Flameng, W.; Petré, C.; Bosman, H.; Yu, J.; Ebert, W.; Hilger, C.S.; Pfefferer, D.; Semmler, W.; Baert, A.L. Paramagnetic Metalloporphyrins: Infarct Avid Contrast Agents for Diagnosis of Acute Myocardial Infarction by MRI. Eur. Radiol. **1996**, *6*, 2–8.
72. Pislaru, S.V.; Ni, Y.; Pislaru, C.; Bosmans, H.; Miao, Y.; Bogaert, J.; Dymarkowski, S.; Semmler, W.; Marchal, G.; Van de Werf, F.J. Noninvasive Measurements of Infarct Size After Thrombolysis With a Necrosis-Avid MRI Contrast Agent. Circulation **1999**, *99*, 690–696.
73. Saeed, M.; Wagner, S.; Wendland, M.F.; Derugin, N.; Finkbeiner, W.E.; Higgins, C.B. Occlusive and Reperfused Myocardial Infarcts: Differentiation With Mn-DPDP-Enhanced MR Imaging. Radiology **1989**, *172*, 59–64.
74. Gallez, B.; Bacic, G.; Swartz, H.M. Evidence for the Dissociation of the Hepatobiliary MRI Contrast Agent Mn-DPDP. Magn. Reson. Med. **1996**, *35*, 14–19.
75. Chauncey, D.M.; Schelbert, H.R.; Halpern, S.E.; Delano, F.; McKegney, M.L.; Ashburn, W.L.; Hagan, P.L. Tissue Distribution Studies With Radioactive Manganese: A Potential Agent for Myocardial Imaging. J. Nucl. Med. **1977**, *18*, 933–936.
76. Vander Elst, L.; Colet, J.M.; Muller, R.N. Spectroscopic and Metabolic Effects of MnCl2 and MnDPDP on the Isolated and Perfused Rat Heart. Invest. Radiol. **1997**, *32*, 581–588.
77. Bremerich, J.; Saeed, M.; Arheden, H.; Higgins, C.B.; Wendland, M.F. Normal and Infarcted Myocardium: Differentiation With Cellular Uptake of Manganese at MR Imaging in a Rat Model. Radiology **2000**, *216*, 524–530.

Received May 24, 2000
Accepted January 11, 2001

MARCEL DEKKER, INC.
270 Madison Avenue, New York, New York 10016